Characterization of Cu_3SbS_3 thin films grown by thermally diffusing Cu_2S and Sb_2S_3 layers

Arshad Hussain[1, 2,*], R. Ahmed[1,**], N. Ali[1], A. Shaari[1], Jing-Ting Luo[2, 3], Yong Qing Fu [2,***]

[1]Department of Physics, Faculty of Science, Universiti Teknologi Malaysia, UTM Skudai, 81310 Johor, Malaysia
[2]Faculty of Engineering & Environment, Northumbria University, Newcastle upon Tyne, NE1 8ST, UK
[3] Institute of Thin Film Physics and Application, Shenzhen University, 518060, China

Corresponding authors: [*]harshad.utm@gmail.com (Arshad Hussain)

[**] rashidahmed@utm.my (Rashid Ahmed)

[***] richard.fu@northumbria.ac.uk (Richard Fu)

Abstract

Copper antimony sulphide (Cu_3SbS_3) with a p-type conductivity and optical band gaps in the range of 1.38 to 1.84 eV is considered to be a promising solar harvesting material with non-toxic and economical elements. In this study, we reported the fabrication of Cu_3SbS_3 thin films using successive thermal evaporation of Cu_2S and Sb_2S_3 layers followed by annealing in an argon atmosphere at a temperature range of 300-375°C. The structural and optical properties of the as-deposited and annealed films were investigated. The annealed films notably show the crystalline phase of the Cu_3SbS_3, identified from the X-ray diffraction analysis and endorsed by the Raman analysis as well. Whereas their chemical state of the constituent elements was characterized with X-ray photoelectron spectroscopy. The measured highest resistivity of the annealed film was found to be ~0.2 Ω-cm. Hence, our obtained results for the fabricated Cu_3SbS_3 thin films bring to light that Cu_3SbS_3would be a good absorber layer in solar cells due to their low resistivity, a higher value of the optical absorption coefficient (~10^5 cm^{-1}), the low transmittance (<5%) and an optical direct band gap of 1.6 eV in the visible range of the solar spectrum.

Keywords: Thin films, Copper antimony sulphide, XRD, Optical properties, Resistivity

1. Introduction

Chalcogenide thin film materials are one of the unique types of the semiconductor compounds which offer broad range applications. In their simplest forms, the chalcogenides are a combination of metal alloys and sulfur, selenium, and tellurium elements, and used for a variety of technological applications including non-volatile phase change memory devices [1] and thin film photovoltaic (PV) devices. The copper based chalcogenide thin films including $Cu_2ZnSnSSe_4$ (CZTSSe, kesterite), $CuSbS_2$ (chalcostibite) and Cu_3BiS_3 (Wittichenite) comprise abundant, low cost and non-toxic elements with a p-type conductivity, and are extensively investigated as an absorber layer for solar cells. These materials are also under extensive research due to their environment-friendly response and appropriate characteristics to harvest the solar energy [2-7]. Colombara et al studied thermochemical and kinetic aspects of the $CuSbS_2$ and Cu_3BiS_3 produced by the conversion of the stacked and co-electroplated metal precursors in the presence of sulfur vapors [8]. Recently different phases of copper antimony sulfide systems are explored as alternatives to the conventional thin film solar cell materials, including Copper indium gallium selenide (CIGS), cadmium telluride (CdTe) and copper zinc tin sulfide (CZTS) [9-11], owing to the fact that copper antimony sulfide contains non-toxic, sustainable constituent elements, and has high absorption coefficient values (~ 10^5 cm^{-1}) [9, 12].

In the literature, fabrication of the copper antimony sulfide thin films are found using both physical and chemical deposition techniques such has thermal evaporation [13-15], thermal diffusion [16], spin coating [17], chemical bath deposition [18], spray pyrolysis [19], electrochemical deposition [20, 21] and hybrid inks method [22], etc. For example, Rabhi et al reported the copper antimony sulfide films fabricated via a thermal evaporation technique [13, 14]. In their work, the value of the optical band gap energy values is reported in the range of 1.8-2.0 eV for the films annealed at temperatures below 200°C, and 1.3 eV for those annealed above this temperature. Together with a p-type conductivity, they mentioned it a suitable material for the absorber layer in solar cells. Similarly, Colombara et al also observed the p-type conductivity with an optical band gap of 1.5eV for the $CuSbS_2$ thin films, prepared using sulfurizing of evaporated Sb-Cu metal stacked layers in a quartz furnace [23], but their reported external quantum efficiency (EQE) of the sulfurized samples was found too low for the application of photovoltaic cells. Their further work also shows that the Sb-rich samples may lead to the desired stoichiometry and enhanced performance of this material in solar cells [23].

Among the different phases of Cu-Sb-S system, most of the studies were focused on the layered orthorhombic structure, $CuSbS_2$ [24, 25]. In a recent theoretical study, the $CuSbS_2$ phase has been predicted as an indirect band gap with a low hole mobility, suggesting it unlikely to achieve the desired transport properties for using it photovoltaics [9, 10]. Additionally, their theoretical study suggests that Cu_3SbS_3 could be preferred if it exhibits the requisite optical and transport characteristics [10]. In the follow-up study, recently Nefzi et al. [26] reported the fabrication of Cu_3SbS_3 thin films by direct melting of the precursor elements and obtained an optical band gap of 1.46 eV with an absorption coefficient of ($\sim 10^5$ cm^{-1}) and a p-type conductivity. In another report, Cu_3SbS_3 thin films prepared by chalcogenization of Cu-Sb precursors have been reported with an optical band gap of 1.84 eV [27]. In a theoretical study, direct band gap energy of the Cu_3SbS_3 thin films was reported to be 2.14 eV [28]. Although the reported studies point to the appropriateness of the Cu_3SbS_3 for solar cell absorber layer, the disparity among different studies is obvious from the reported data. Therefore, to comprehend its potential as an absorber layer for solar cell applications, further studies of its material properties are urgently needed.

In this study, we propose a simple, cost-effective, robust and environment-friendly thermal evaporation method, in which the precursors of Cu_2S and Sb_2S_3 layers were directly evaporated onto substrates, followed by thermally annealing and inter-diffusing of the two layers in an argon atmosphere at different temperatures (300-375 °C) for 60 minutes. Effects of annealing temperatures on the structural and optical properties of the samples are investigated.

2. Experimental details

Thin films of Cu_3SbS_3 were deposited ultrasonically on cleaned soda lime glass substrates using a single source thermal evaporation system (Edward 306) by evaporating Cu_2S and Sb_2S_3 powder precursors acquired from Sigma-Aldrich with 99.999% purity. A 400-nm thick layer of Sb_2S_3 was firstly evaporated onto the glass substrates followed by a 170-nm thick Cu_2S layer, all in a high vacuum (with a base vacuum of $\sim 10^{-6}$ mbar). After the deposition, the two layers were inter-diffused by annealing the as-deposited films at various temperatures of 300, 325, 350 and 375 °C in a quartz tube furnace in an argon atmosphere for 60 min to study the effect of annealing on the film properties.

The as-deposited and annealed samples were investigated using different characterization techniques. The crystalline structures of the films were characterized using x-ray diffraction (XRD) analysis with a D500 Siemens diffractometer and Cu Kα radiation (λ=1.54 Å). Raman spectra measurement was performed using a Renishaw Via Raman spectrometer with an Ar^+ laser excitation source (514.5 nm). Morphological features of the obtained samples were studied using atomic force microscopy (AFM, Seiko Instrument, SPA-300HV). The scanning electron microscope (SEM, JEOL JSM 6380la) with attached energy dispersive X-ray spectroscopy (EDX) unit was used to study the cross-sectional morphology and elemental composition of the fabricated samples. X-ray photoelectron spectroscopic (XPS) analysis was also performed using Kratos Axis Ultra X-ray photoelectron spectrometer with Al K_α radiation (1486.6 eV) source, for composition and chemical state analysis. UV-Vis spectrophotometer (UV-3101PC) was used to investigate the optical properties of the samples. A Keithley 2400 source meter attached with 4-probes was used to obtain the I-V characteristics and electrical resistance measurements. The electrical contacts were made on thin film surface using adhesive silver conductive paint and the measurements were performed by gradually increasing the applied voltage up to 6 V.

3. Results and discussion

Figure 1 displays the XRD patterns of the as-deposited and annealed (300-375 °C) thin film samples. From Fig. 1, the peak intensities are observed to be enhanced with increasing annealing temperature, and the sharper peaks for the samples annealed at higher temperatures indicate that their crystalline quality has been sufficiently improved. The phases of the obtained samples were identified using the PDF standard cards (26-1110, 71-0555). Most of the peaks can be assigned to the skinnerite monoclinic Cu_3SbS_3 phase, however, there are a few lower intensity peaks corresponding to Cu_3SbS_4 phase (PDF# 71-0555) as indicated in Fig. 1. The results are consistent with the previous reports in the literature [9, 27]. The crystallite sizes of the samples were estimated using the well-known Scherrer's equation [15, 29-31], based on the (2 1 2) crystalline peak of Cu_3SbS_3 phase:

$$D = \frac{0.9\lambda}{\beta \cos\theta} \qquad (1)$$

where D is the crystallite size, λ is the wavelength of the x-rays source used, β is the peak width at half maximum (FWHM) and θ is the diffraction Bragg's angle. The dependence of crystallite

size on annealing temperature is shown in Fig 2. The measured crystallite size is in the range between 27 to 53 nm and is found to increase with the annealing temperature [32].

Fig. 3 showed the Raman spectra of Cu_3SbS_3 samples annealed at various temperatures ranging from 300 to 375°C. As evident from the spectra, the fabricated samples show Raman active modes at 128, 153, 190, 238, 308 and 351 cm^{-1}. The observed Raman modes at 308 and 351 are corresponding to those of Cu_3SbS_3 phase [33]. Weak modes observed at 128 and 190 cm^{-1} are corresponding to that of $CuSbS_2$ [34], however, the relatively low peaks are only appeared in low temperature annealed film but not in the 375°C annealed sample. The nonappearance of any peak of $CuSbS_2$ phase in XRD pattern of the obtained samples might be due to its existence in a small amount. A mode found at 280 cm^{-1} is close to that of Cu_3SbS_4 phase [35], and the intensity of this mode is gradually decreasing with annealing temperature which is consistent with the XRD pattern. There was one other mode at 153 cm^{-1} which is appeared at higher annealing temperatures is not matched with any of the binary phases such as Cu_xS or Sb_2S_3 and ternary phases such as Cu_3SbS_4, $CuSbS_2$ or $Cu_{12}Sb_4S_{13}$ [36]. From the XRD analysis the dominant phase is Cu_3SbS_3, therefore we may attribute this mode to Cu_3SbS_3 phase. The dominant modes of Raman spectra are mostly due to a Cu_3SbS_3 phase which is also revealed by XRD pattern of these samples.

Morphological characteristics of the fabricated Cu_3SbS_3 thin films were demonstrated using the AFM micrographs as displayed in Figs 4 (a-d) corresponding to the samples annealed at 300-375 °C respectively. Spherical grains of diameter 10-40 nm (300 °C annealed sample), 20-40 nm (325 °C annealed sample), 30-50 nm (350 °C annealed sample) and 30-60 nm (375 °C annealed sample) respectively were obtained from the images. As evident from the Fig 4 (a-d), densely packed grains can be observed in all the samples with well-defined grain boundaries. The surface roughness data from RMS roughness analysis were obtained and found to be decreased from 9.26 to 4.23 as the annealing temperature was increased from 300 to 375 °C.

Figure 5 and inset represent the cross-sectional images of the as-deposited and 375 °C annealed samples respectively. Two layers of Cu_2S and Sb_2S_3 of thicknesses 176 and 400 nm can be seen in Fig 5, with a total thickness of 576 nm for the thin film. The annealing results in a uniform single layer as shown in the inset of Fig. 5 for the Cu_3SbS_3 thin film of 500 nm thickness without apparent holes or voids, representing a good adhesion with the substrate. Moreover, EDX analysis also showed the atomic percentage of the elements Cu, Sb, and S 41.5 at%, 15.5 at%, and 40.5 at%, respectively.

The results of chemical element compositions for the Cu_3SbS_3 thin film (350°C annealed) were obtained from XPS analysis and the results are shown in Fig. 6. The peak of C1s was used as a reference to correct the peak shift due to charging or other effects. The high-resolution core level spectra of the above-identified three elements along with the de-convoluted ones (dotted lines) are shown in Figs. 7. (a-c). The core level spectrum of the copper reveals a 2p doublet state as shown in Fig. 7 (a), at binding energies of 929.7 and 930.7 eV corresponding to Cu $2p_{3/2}$ and 949.5 and 950.3 eV corresponding to Cu $2p_{1/2}$, respectively, with a peak separation of 19.8 eV. The higher intensity peak corresponds to Cu-S bonding while the lower intensity peak is linked to Cu-O. The concentration of each peak to the main peaks are 54.9%, 13.7%, 21.2% and 10.0% respectively, with the peak areas 4411, 1107, 1707, and 804 as calculated from CasaXPS software. Thus, the ratio between the two peaks (Cu-S: Cu-O) is estimated to be ~3:1, indicating the first binding peak (Cu-S) is dominant on the film surface. The existence of Cu-O is mainly from the surface adsorption from the atmosphere, and a small amount of Cu-O could be also from the residue oxygen in the chamber. Fig. 7 (b) shows the high-resolution spectra for $Sb_{5/2}$ and $Sb_{3/2}$ core levels along with the deconvoluted plots. The main peaks of Sb are observed at binding energies 529.1 and 537.1 eV with a peak separation of 8.0 eV as shown in Fig. 7 (b). The main peaks at binding energies 529.1 eV and 537.1 eV corresponds to Sb-S chemical bonding, similar to those at 527.7 eV and 536.2 for Cu-Sb-S. The smaller peaks at 530.1 eV and 537.6 correspond to Sb-O, with a small concentration of about ~4% from surface adsorption. However, the intensity of the peaks is corresponding to the concentrations of ~65% and 25%, with the peak areas (relative sensitivity factor (RSF) corrected intensities) of 901.9, 2197.8, 1450.6 and 520.2 from lower to higher binding energies respectively. The S 2p core level and corresponding deconvoluted spectra (Fig. 7 (c)) show four distinct peaks at binding energies of 158.9, 160.3 and 161.7 eV. The concentration of

each peak in the main peaks is 25.7%, 38.0%, and 15.1% respectively, with peak areas of 3971, 747, 5612 and 2933, corresponding to S-Sb, S-Cu, and S-O chemical bonding respectively from lower to higher binding energies. The values of the binding energies for S 2p are consistent with the range for S in sulphide phases [37]. All the corresponding binding energy values of the elements of Cu_3SbS_3 were found consistent with those in the literature [3, 17, 38].

The optical transmission and reflection spectra of the films were examined in the wavelength range of 200-1600 nm at room temperature, and the results are displayed in Figs. 8 (a) and (b) respectively. It can be observed from Fig. 8 (a) that the transmittance of the obtained film is minimum in the visible region of the solar spectrum and then starts to increase beyond the visible region up to 800 nm and finally decreases at a larger wavelength. The transmittance of the film annealed at 375°C shows the lowest transmittance (<5%), representing the highest absorption capacity of the obtained Cu_3SbS_3 thin film samples. The transition from ~900 to 700 nm in the transmittance spectra of the films annealed at a temperature below 375°C might be due to the absorption of Cu_3SbS_4 phase [35], which is also found in the reflectance spectra (Fig. 8 (b)). But this transition disappears in the film annealed at 375°C both in transmittance and reflectance spectra indicating the reduction of the impurity phase in the sample. The reflectance of the obtained samples is about 10-35% which is evident from Fig 8 (b). The optical absorption coefficients of the thin films were obtained using the transmittance and reflection data based on the following equation [15, 26];

$$\alpha = \frac{1}{d}\left[\frac{(1-R^2)}{2T} + \left(\frac{(1-R^4)}{4T^2}\right) + R^2\right] \quad (2)$$

where α is the absorption coefficient, d is the thickness of the film, T, and R are the transmission and reflection spectra, respectively.

The absorption coefficients of the annealed samples are in the order of ~10^5 cm^{-1} in the visible region of the solar spectra as shown in Fig. 9 (a). This high absorption property makes the obtained Cu_3SbS_3 thin film a suitable candidate for the absorber layer in solar cells.

The energy band gap E_g of the fabricated films can be obtained by the Tauc's equation based on the data from Fig. 9 (b) [39, 40],

$$\alpha h\nu = A\,(h\nu - Eg)^n \qquad (3)$$

where α is the absorption co-efficient, $h\nu$ is the photon energy, A is an energy dependent constant, $n = 2$ for direct and $n = 1/2$ indirect allowed transitions, respectively. The Tauc's plots for the optical band gap of the obtained thin films are shown in Fig 9 (b). The calculated band gap values for the fabricated samples are in the range 1.6 to 1.8 eV. The sample annealed at 375°C showed the band gap energy values of 1.6±0.1 eV, which is in close proximity to the optimum value for the absorber material. Therefore, the prepared Cu_3SbS_3 can be considered as a good absorber material for the solar cell applications.

The current-voltage characteristics of the annealed films at 300-375°C are shown in Fig. 10. It is evident from the plots that the variation of the current with the voltage is linear and the current is observed to increase linearly with the annealing temperature, which can be attributed to the enhancement of the crystalline quality and decrease of the grain boundaries. The resistivity of the samples obtained from the I-V characteristic curves is observed to decrease with increasing annealing temperature as shown in Fig 11, hence the increase in electrical conductivity at higher temperature may be attributed to the reduction of potential barriers generated by the grain boundaries thus resulting in an increase in the electrical conductivity of the films [41, 42]. Moreover, the conductivity of this material is reported as p-type [26, 27], which highlights the suitability of this material for the absorber layer in solar cells.

From structural, morphological and optoelectronic analyses of the obtained Cu_3SbS_3 thin films, it is evident that the annealing temperature improved these properties of the films. No peak shifting in Cu_3SbS_3 XRD pattern was observed with increasing annealing temperature from 300 to 400°C. The intensity of the diffraction peaks was found to increase and their broadening decreased with increasing annealing temperature. These indicate the enhancement in the crystalline quality and crystallite size of the obtained samples, which are also confirmed by AFM analysis. Similarly, the optoelectronic properties of the fabricated samples were found to improve with increasing

annealing temperature. Enhancement in the electrical conductivity can be attributed to increasing the crystalline quality and reduction of the potential barriers with increasing temperature.

4. Conclusion

Thin films of the Cu_3SbS_3 were fabricated by thermally evaporated Cu_2S and Sb_2S_3 layers in a high vacuum. The fabricated samples were annealed, in an argon atmosphere, at temperatures ranging from 300-375°C, and the effect of annealing on various properties of the samples was studied. XRD analysis revealed that the samples were crystalline with skinnerite monoclinic Cu_3SbS_3 structure which was confirmed by Raman analysis of the samples as well. The crystallinity was observed to improve with increasing annealing temperature. The average crystallite size calculated from the Scherrer's equation was found to be 27 to 53 nm. The value of the optical absorption coefficients of the fabricated films (~10^5 cm^{-1}) and the optical energy band gap of 1.6 ± 0.1 eV in the visible range of the solar spectrum, showed the appropriateness of Cu_3SbS_3 thin films for the absorber layer in solar cells.

Acknowledgements

The authors would like to thank University Teknologi Malaysia/Ministry of Education Malaysia for the financial support of this research work through project nos. Q.J130000.2526.12H46, R.J130000.7826.4F508, and International Doctoral Fellowship/UTM IDF.

References

[1] Y. Jung, R. Agarwal, C.-Y. Yang, R. Agarwal, Chalcogenide phase-change memory nanotubes for lower writing current operation, Nanotechnology, 22 (2011) 254012.
[2] B. Krishnan, S. Shaji, R.E. Ornelas, Progress in the development of copper antimony sulfide thin films as an alternative material for solar energy harvesting, Journal of Materials Science: Materials in Electronics, 26 (2015) 4770-4781.
[3] R. Ornelas-Acosta, S. Shaji, D. Avellaneda, G. Castillo, T.D. Roy, B. Krishnan, Thin films of copper antimony sulfide: a photovoltaic absorber material, Materials Research Bulletin, 61 (2015) 215-225.
[4] W.-L. Chen, D.-H. Kuo, T.T.A. Tuan, Preparation of CuSbS2 Thin Films by Co-Sputtering and Solar Cell Devices with Band Gap-Adjustable n-Type InGaN as a Substitute of ZnO, Journal of Electronic Materials, 45 (2016) 688-694.
[5] M. Kumar, C. Persson, Cu3BiS3 as a potential photovoltaic absorber with high optical efficiency, Applied Physics Letters, 102 (2013) 062109.

[6] A. Hussain, R. Ahmed, N. Ali, F.K. Butt, A. Shaari, W.W. Shamsuri, R. Khenata, D. Prakash, K. Verma, Post-annealing effects on structural, optical and electrical properties of CuSbS 2 thin films fabricated by combinatorial thermal evaporation technique, Superlattices and Microstructures, 89 (2016) 136-144.
[7] S.A. Vanalakar, G.L. Agawane, S.W. Shin, M.P. Suryawanshi, K.V. Gurav, K.S. Jeon, P.S. Patil, C.W. Jeong, J.Y. Kim, J.H. Kim, A review on pulsed laser deposited CZTS thin films for solar cell applications, Journal of Alloys and Compounds, 619 (2015) 109-121.
[8] D. Colombara, L.M. Peter, K.D. Rogers, K. Hutchings, Thermochemical and kinetic aspects of the sulfurization of Cu–Sb and Cu–Bi thin films, Journal of Solid State Chemistry, 186 (2012) 36-46.
[9] K. Ramasamy, H. Sims, W.H. Butler, A. Gupta, Selective nanocrystal synthesis and calculated electronic structure of all four phases of copper–antimony–sulfide, Chemistry of Materials, 26 (2014) 2891-2899.
[10] D.J. Temple, A.B. Kehoe, J.P. Allen, G.W. Watson, D.O. Scanlon, Geometry, electronic structure, and bonding in CuMCh2 (M= Sb, Bi; Ch= S, Se): alternative solar cell absorber materials?, The Journal of Physical Chemistry C, 116 (2012) 7334-7340.
[11] C. Yan, Z. Su, E. Gu, T. Cao, J. Yang, J. Liu, F. Liu, Y. Lai, J. Li, Y. Liu, Solution-based synthesis of chalcostibite (CuSbS 2) nanobricks for solar energy conversion, RSC Advances, 2 (2012) 10481-10484.
[12] J. van Embden, K. Latham, N.W. Duffy, Y. Tachibana, Near-infrared absorbing Cu12Sb4S13 and Cu3SbS4 nanocrystals: synthesis, characterization, and photoelectrochemistry, Journal of the American Chemical Society, 135 (2013) 11562-11571.
[13] A. Rabhi, M. Kanzari, B. Rezig, Growth and vacuum post-annealing effect on the properties of the new absorber CuSbS2 thin films, Materials Letters, 62 (2008) 3576-3578.
[14] A. Rabhi, M. Kanzari, B. Rezig, Optical and structural properties of CuSbS 2 thin films grown by a thermal evaporation method, Thin Solid Films, 517 (2009) 2477-2480.
[15] A. Rabhi, Y. Fadhli, M. Kanzari, Investigation on dispersive optical constants and microstructural parameters of the absorber CuSbS 2 thin films, Vacuum, 112 (2015) 59-65.
[16] C. Garza, S. Shaji, A. Arato, E.P. Tijerina, G.A. Castillo, T.D. Roy, B. Krishnan, p-Type CuSbS 2 thin films by thermal diffusion of copper into Sb 2 S 3, Solar Energy Materials and Solar Cells, 95 (2011) 2001-2005.
[17] B. Yang, L. Wang, J. Han, Y. Zhou, H. Song, S. Chen, J. Zhong, L. Lv, D. Niu, J. Tang, CuSbS2 as a promising earth-abundant photovoltaic absorber material: a combined theoretical and experimental study, Chemistry of Materials, 26 (2014) 3135-3143.
[18] Y. Rodriguez-Lazcano, M. Nair, P. Nair, Photovoltaic pin structure of Sb2S3 and CuSbS2 absorber films obtained via chemical bath deposition, Journal of The Electrochemical Society, 152 (2005) G635-G638.
[19] S. Thiruvenkadam, A.L. Rajesh, Effect Of Antimony Concentration On The Properties Of Spray Pyrolysed Cusbs2 Thin Film Absorbing Layer For Photovoltaic Application, International Journal of Technology Enhancements and Emerging Engineering Research, 3 (2014) 38-41.
[20] W. Septina, S. Ikeda, Y. Iga, T. Harada, M. Matsumura, Thin film solar cell based on CuSbS 2 absorber fabricated from an electrochemically deposited metal stack, Thin Solid Films, 550 (2014) 700-704.
[21] A. Rastogi, N. Janardhana, Properties of CuSbS 2 thin films electrodeposited from ionic liquids as p-type absorber for photovoltaic solar cells, Thin Solid Films, 565 (2014) 285-292.

[22] S. Banu, S.J. Ahn, S.K. Ahn, K. Yoon, A. Cho, Fabrication and characterization of cost-efficient CuSbS 2 thin film solar cells using hybrid inks, Solar Energy Materials and Solar Cells, 151 (2016) 14-23.
[23] D. Colombara, L.M. Peter, K.D. Rogers, J.D. Painter, S. Roncallo, Formation of CuSbS 2 and CuSbSe 2 thin films via chalcogenisation of Sb–Cu metal precursors, Thin Solid Films, 519 (2011) 7438-7443.
[24] M. Kumar, C. Persson, CuSbS2 and CuBiS2 as potential absorber materials for thin-film solar cells, Journal of Renewable and Sustainable Energy, 5 (2013) 031616.
[25] J.T. Dufton, A. Walsh, P.M. Panchmatia, L.M. Peter, D. Colombara, M.S. Islam, Structural and electronic properties of CuSbS 2 and CuBiS 2: potential absorber materials for thin-film solar cells, Physical Chemistry Chemical Physics, 14 (2012) 7229-7233.
[26] K. Nefzi, A. Rabhi, M. Kanzari, Investigation of physical properties and impedance spectroscopy study of Cu3SbS3 thin films, Journal of Materials Science: Materials in Electronics, DOI 1-9.
[27] P. Maiello, G. Zoppi, R.W. Miles, N. Pearsall, I. Forbes, Chalcogenisation of Cu–Sb metallic precursors into Cu 3 Sb (Se x S 1− x) 3, Solar Energy Materials and Solar Cells, 113 (2013) 186-194.
[28] A.B. Kehoe, D.J. Temple, G.W. Watson, D.O. Scanlon, Cu 3 MCh 3 (M= Sb, Bi; Ch= S, Se) as candidate solar cell absorbers: insights from theory, Physical Chemistry Chemical Physics, 15 (2013) 15477-15484.
[29] Y. Zhang, C. Liao, K. Zong, H. Wang, J. Liu, T. Jiang, J. Han, G. Liu, L. Cui, Q. Ye, H. Yan, W. Lau, Cu2ZnSnSe4 thin film solar cells prepared by rapid thermal annealing of co-electroplated Cu–Zn–Sn precursors, Solar Energy, 94 (2013) 1-7.
[30] J. Lehner, M. Ganchev, M. Loorits, N. Revathi, T. Raadik, J. Raudoja, M. Grossberg, E. Mellikov, O. Volobujeva, Structural and compositional properties of CZTS thin films formed by rapid thermal annealing of electrodeposited layers, Journal of Crystal Growth, 380 (2013) 236-240.
[31] S.G. Lee, J. Kim, H.S. Woo, Y. Jo, A.I. Inamdar, S.M. Pawar, H.S. Kim, W. Jung, H.S. Im, Structural, morphological, compositional, and optical properties of single step electrodeposited Cu2ZnSnS4 (CZTS) thin films for solar cell application, Current Applied Physics, 14 (2014) 254-258.
[32] S. Chander, M. Dhaka, Impact of thermal annealing on physical properties of vacuum evaporated polycrystalline CdTe thin films for solar cell applications, Physica E: Low-dimensional Systems and Nanostructures, 80 (2016) 62-68.
[33] X. Qiu, S. Ji, C. Chen, G. Liu, C. Ye, Synthesis, characterization, and surface-enhanced Raman scattering of near infrared absorbing Cu 3 SbS 3 nanocrystals, CrystEngComm, 15 (2013) 10431-10434.
[34] V. Vinayakumar, S. Shaji, D. Avellaneda, T.D. Roy, G. Castillo, J. Martinez, B. Krishnan, CuSbS 2 thin films by rapid thermal processing of Sb 2 S 3-Cu stack layers for photovoltaic application, Solar Energy Materials and Solar Cells, 164 (2017) 19-27.
[35] U. Chalapathi, B. Poornaprakash, S.-H. Park, Growth and properties of Cu 3 SbS 4 thin films prepared by a two-stage process for solar cell applications, Ceramics International, DOI (2017).
[36] R. Downs, The RRUFF Project: an integrated study of the chemistry, crystallography, Raman and infrared spectroscopy of minerals, Program and abstracts of the 19th general meeting of the international mineralogical association in Kobe, Japan, 2006, pp. 13.

[37] X. NIST, Standard Reference Database 20, Version, 2003.
[38] R. Ornelas-Acosta, D. Avellaneda, S. Shaji, G. Castillo, T.D. Roy, B. Krishnan, CuSbS2 thin films by heating Sb2S3/Cu layers for PV applications, Journal of Materials Science: Materials in Electronics, 25 (2014) 4356-4362.
[39] J. Tauc, R. Grigorovici, A. Vancu, Optical Properties and Electronic Structure of Amorphous Germanium, physica status solidi (b), 15 (1966) 627-637.
[40] V. Şenay, S. Özen, S. Pat, Ş. Korkmaz, Optical, structural, morphological and compositional characterization of a Co-doped GaAs semiconducting thin film produced by thermionic vacuum arc, Journal of Alloys and Compounds, 663 (2016) 829-833.
[41] G. Rusu, M. Rusu, On the electrical conductivity of CdTe thin films evaporated onto unheated substrates, Solid State Communications, 116 (2000) 363-368.
[42] N. Ali, A. Hussain, R. Ahmed, M.K. Wang, C. Zhao, B.U. Haq, Y.Q. Fu, Advances in nanostructured thin film materials for solar cell applications, Renewable and Sustainable Energy Reviews, 59 (2016) 726-737.

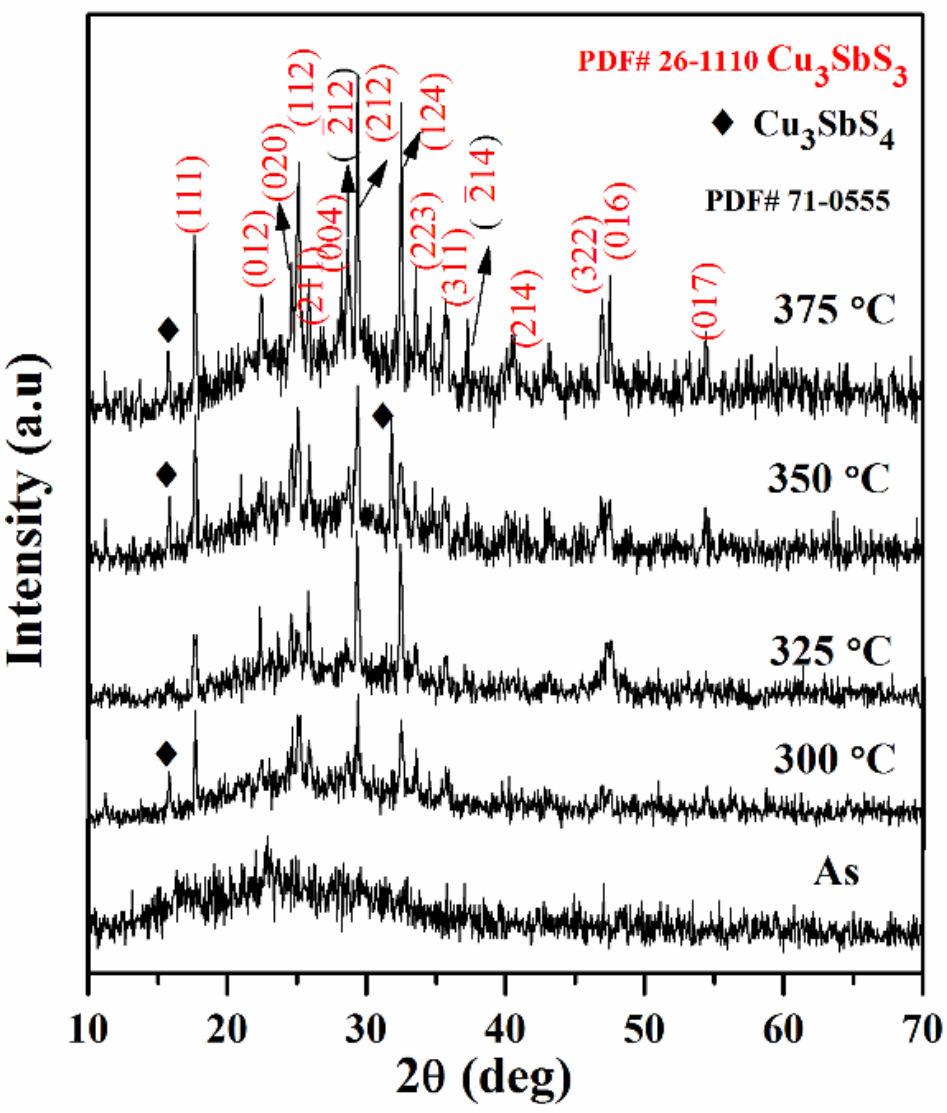

Fig. 1. X-ray diffraction patterns of the as-deposited and annealed Cu_3SbS_3 thin films.

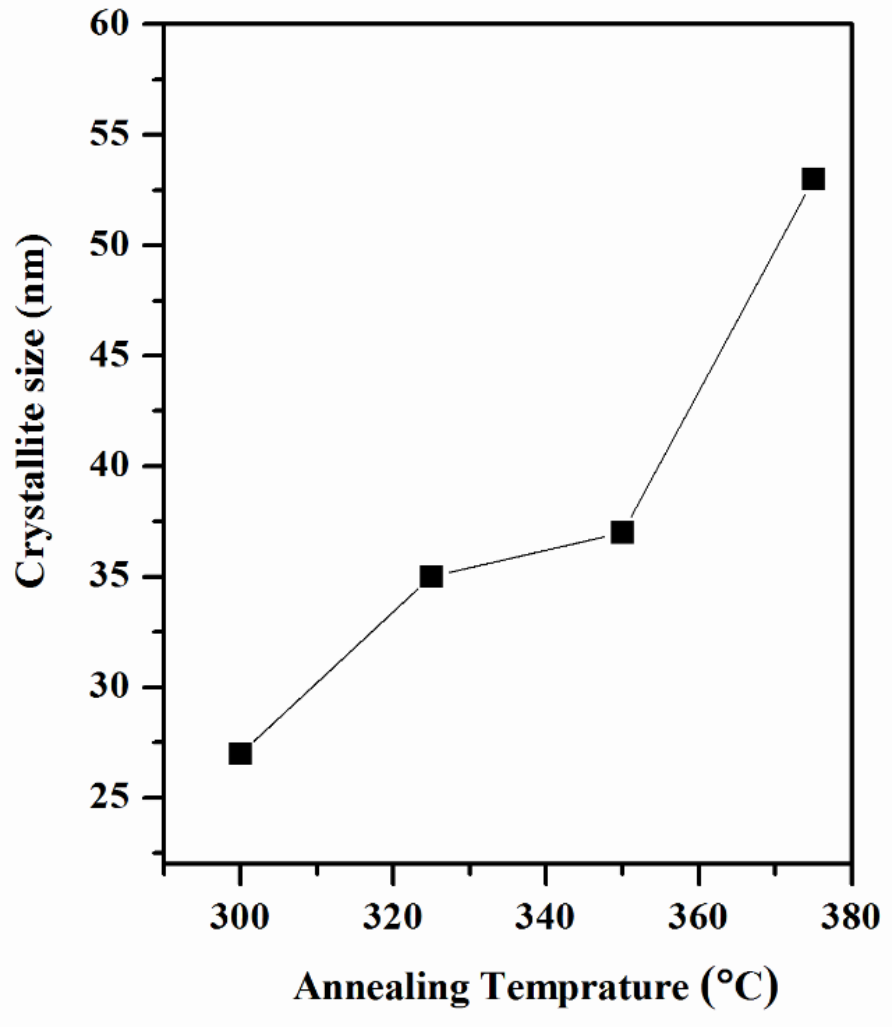

Fig. 2. Crystallite size as a function of annealing temperature obtained from data of (2 1 2) peak of Cu_3SbS_3 samples.

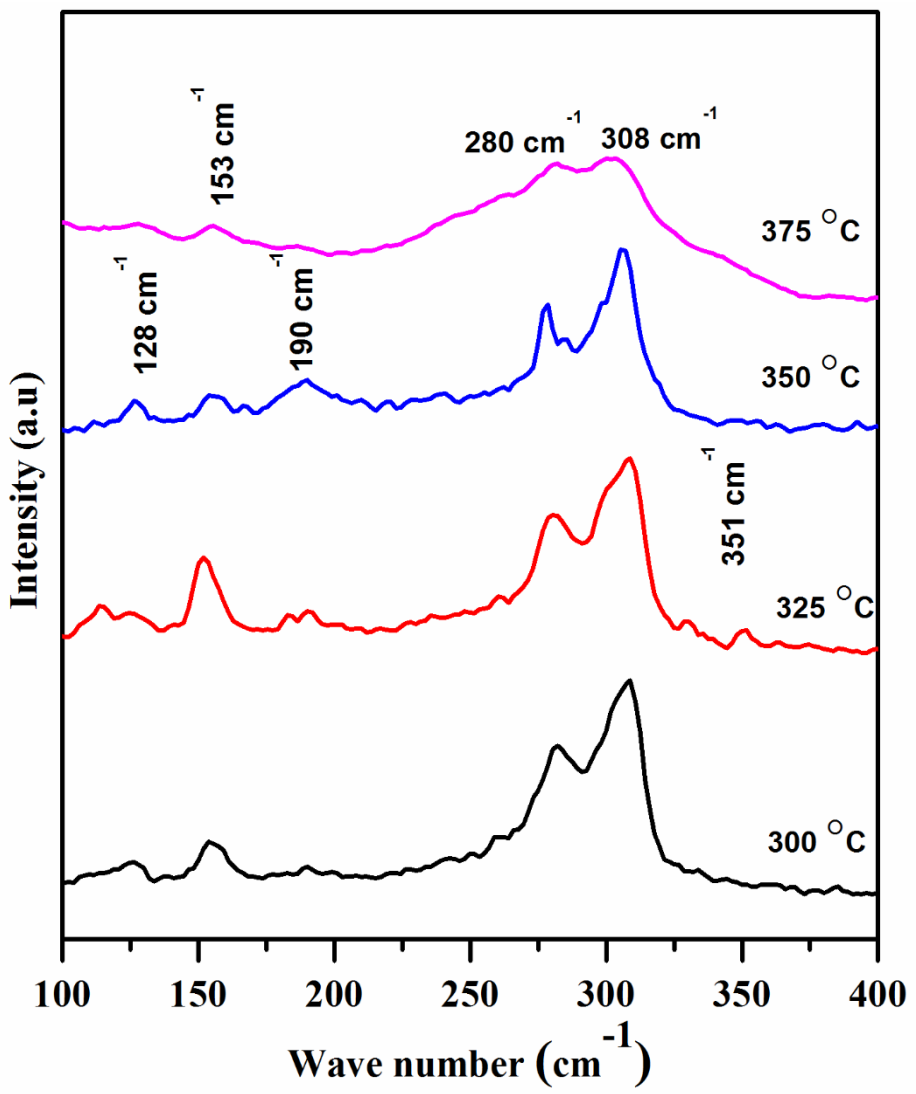

Fig. 3. Raman spectra of Cu_3SbS_3 thin films obtained by thermally diffusing Cu_2S and Sb_2S_3 layers followed by annealing the samples in argon atmosphere at various temperatures, ranging from 300 to 375°C as labeled in the figure.

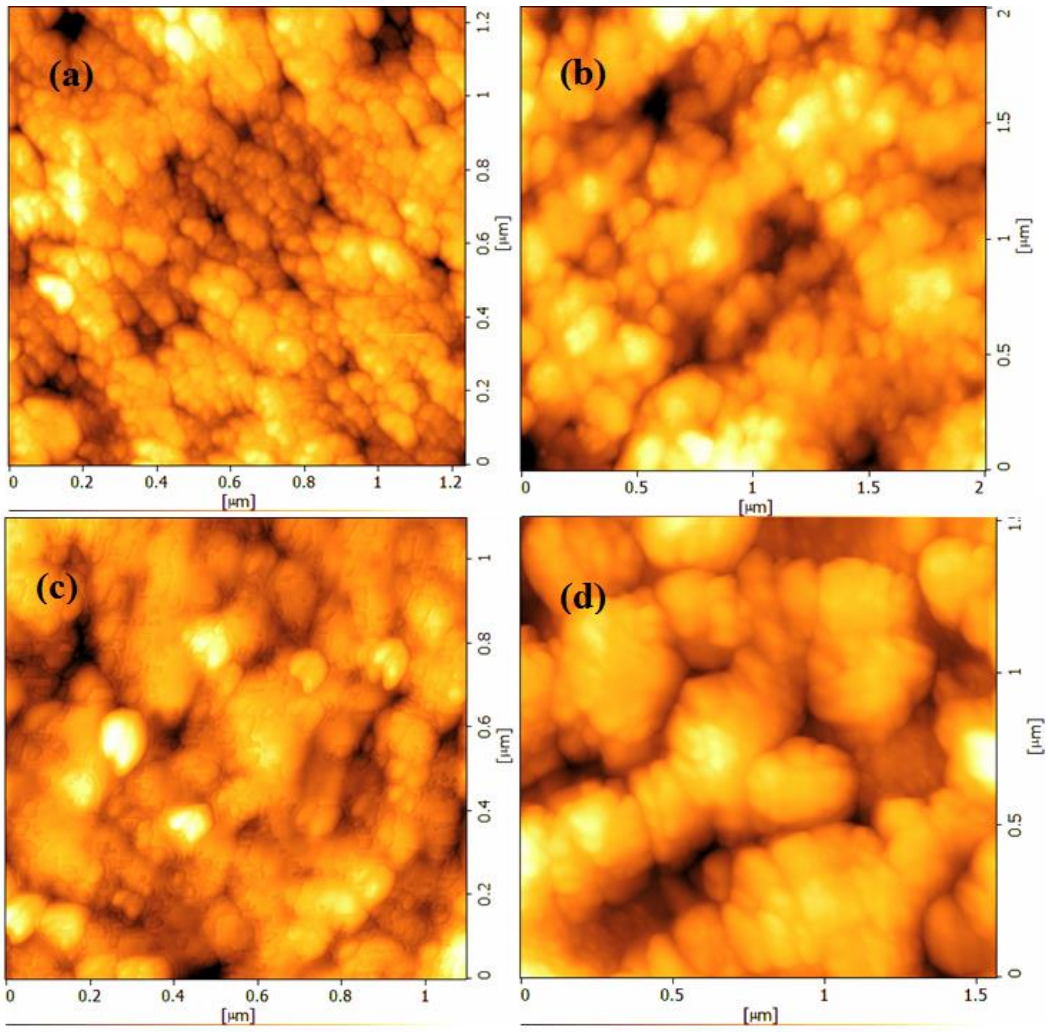

Fig. 4. AFM micrographs of the obtained Cu_3SbS_3 by thermally annealing and diffusing the two Cu_2S and Sb_2S_3 layers in argon atmosphere at temperature (a) 300 ˚C (b) 325 ˚C (c) 350 ˚C (d) 375 ˚C.

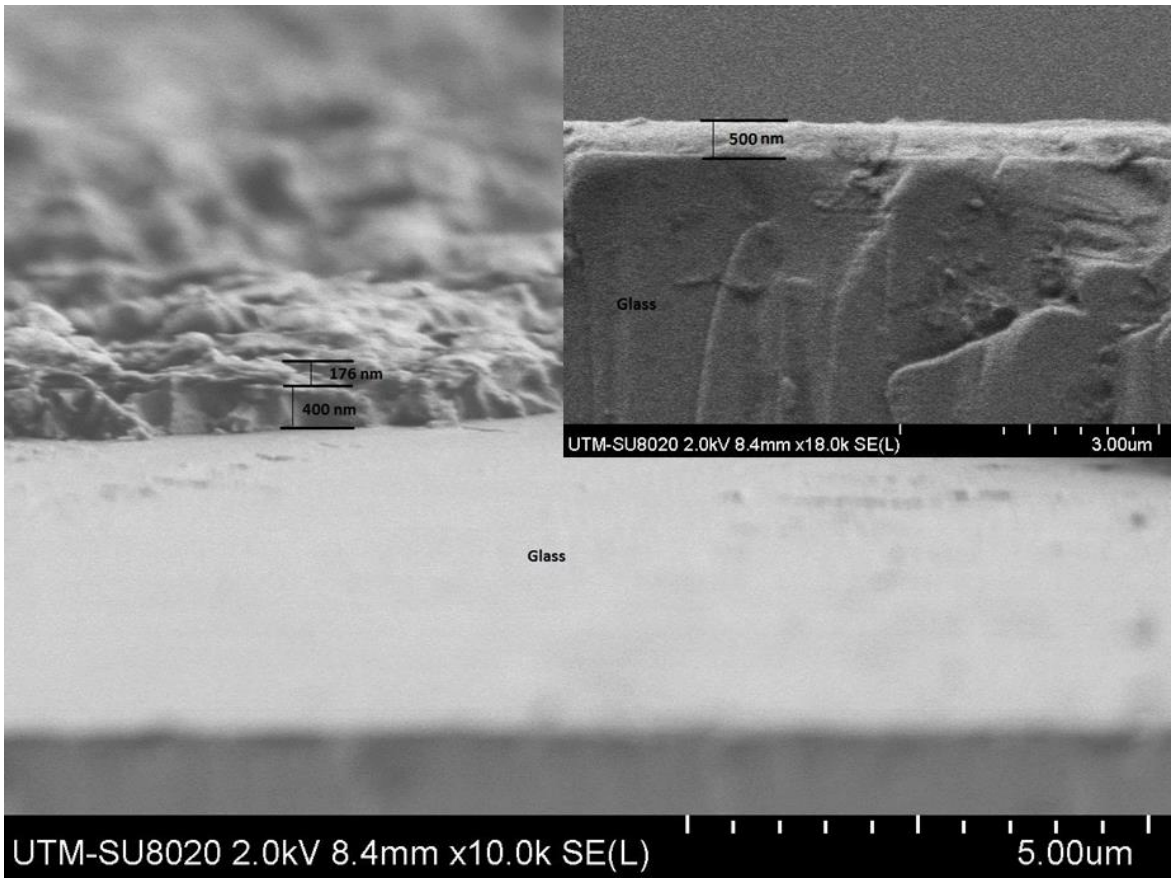

Fig. 5. Cross-sectional SEM image of as-deposited and 375 ˚C annealed sample (inset).

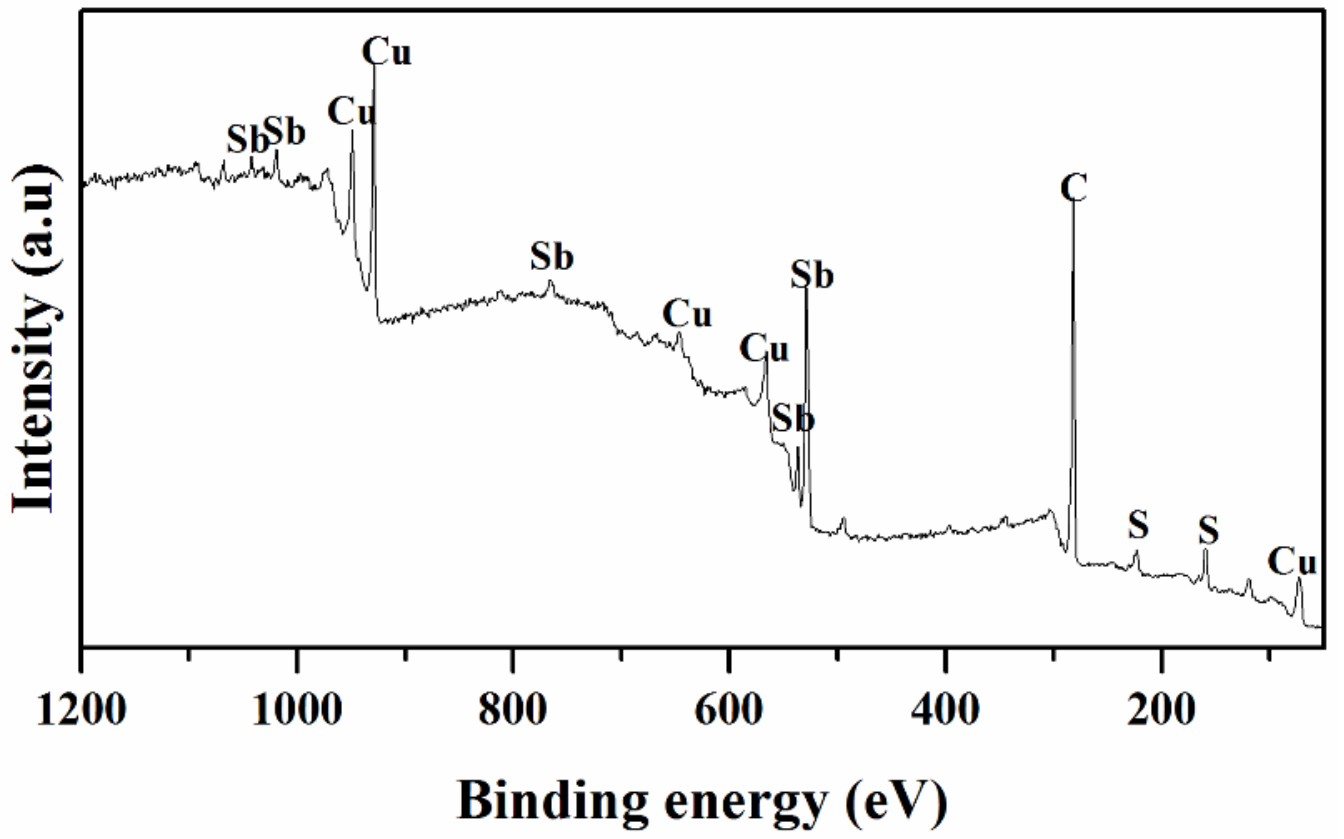

Fig. 6. XPS survey spectra of Cu_3SbS_3 thin film annealed at 375 °C in argon.

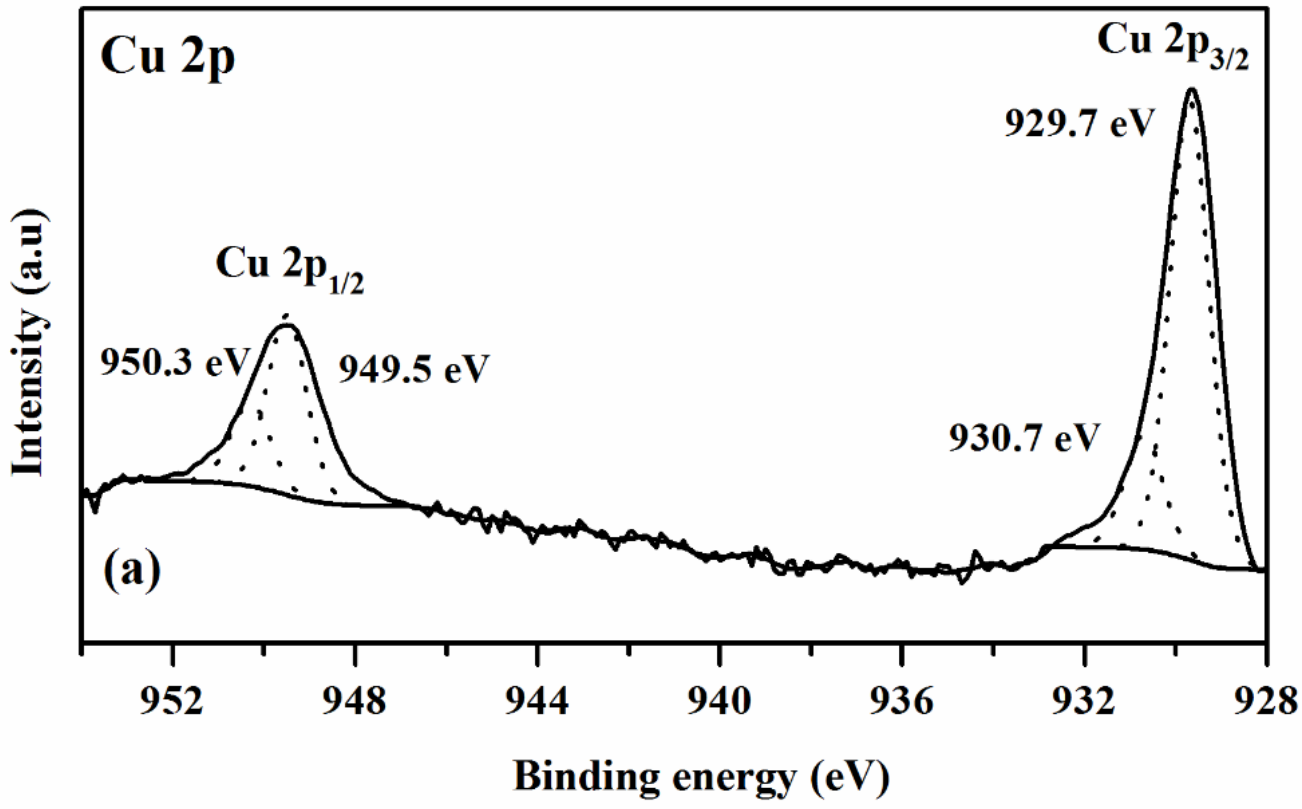
Cu 2p
Cu 2p3/2
929.7 eV
Cu 2p1/2
950.3 eV
949.5 eV
930.7 eV
(a)
Intensity (a.u)
952
948
944
940
936
932
928
Binding energy (eV)

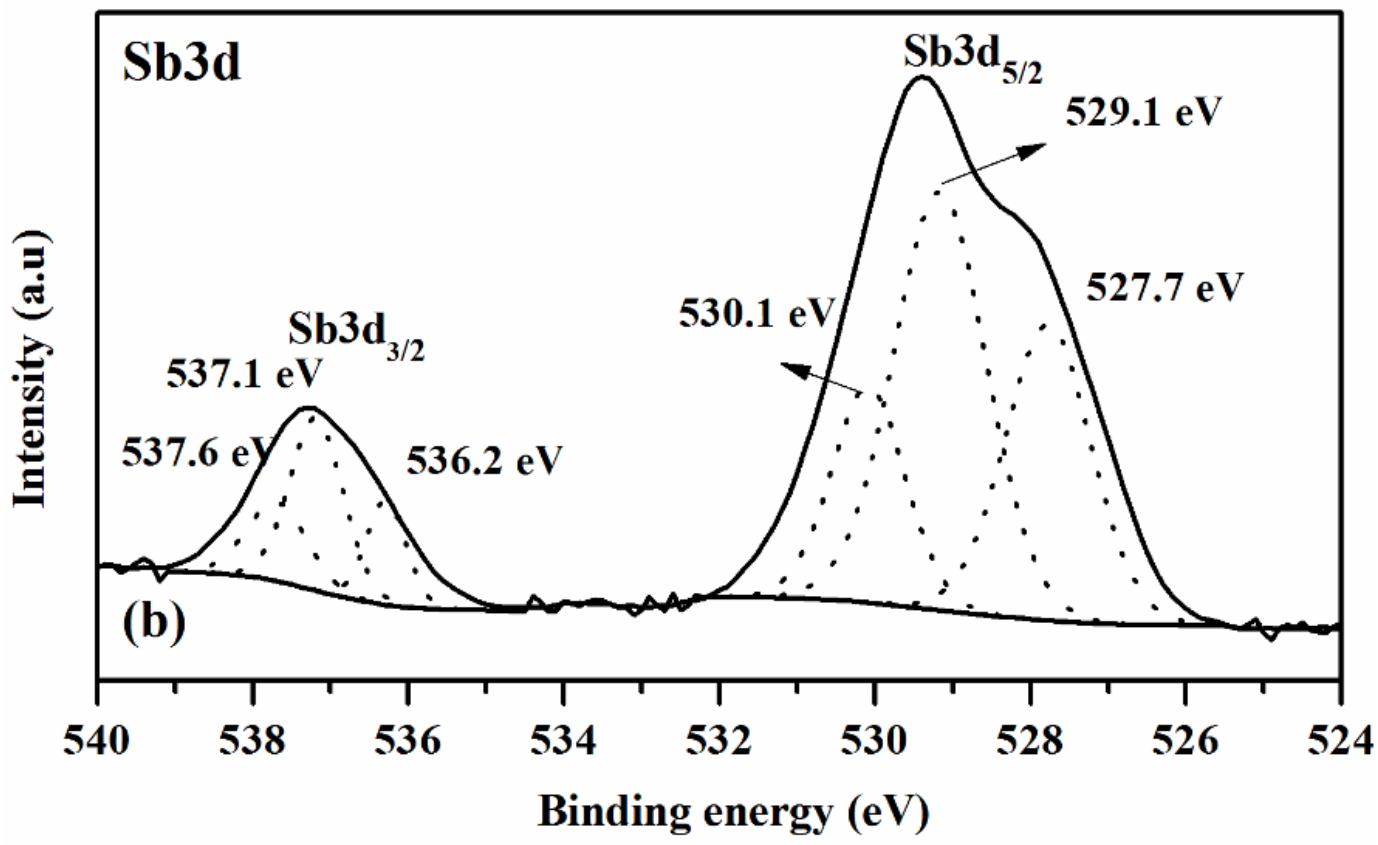
Sb3d
Sb3d5/2
529.1 eV
527.7 eV
530.1 eV
Sb3d3/2
537.1 eV
537.6 eV
536.2 eV
(b)
Intensity (a.u)
540
538
536
534
532
530
528
526
524
Binding energy (eV)

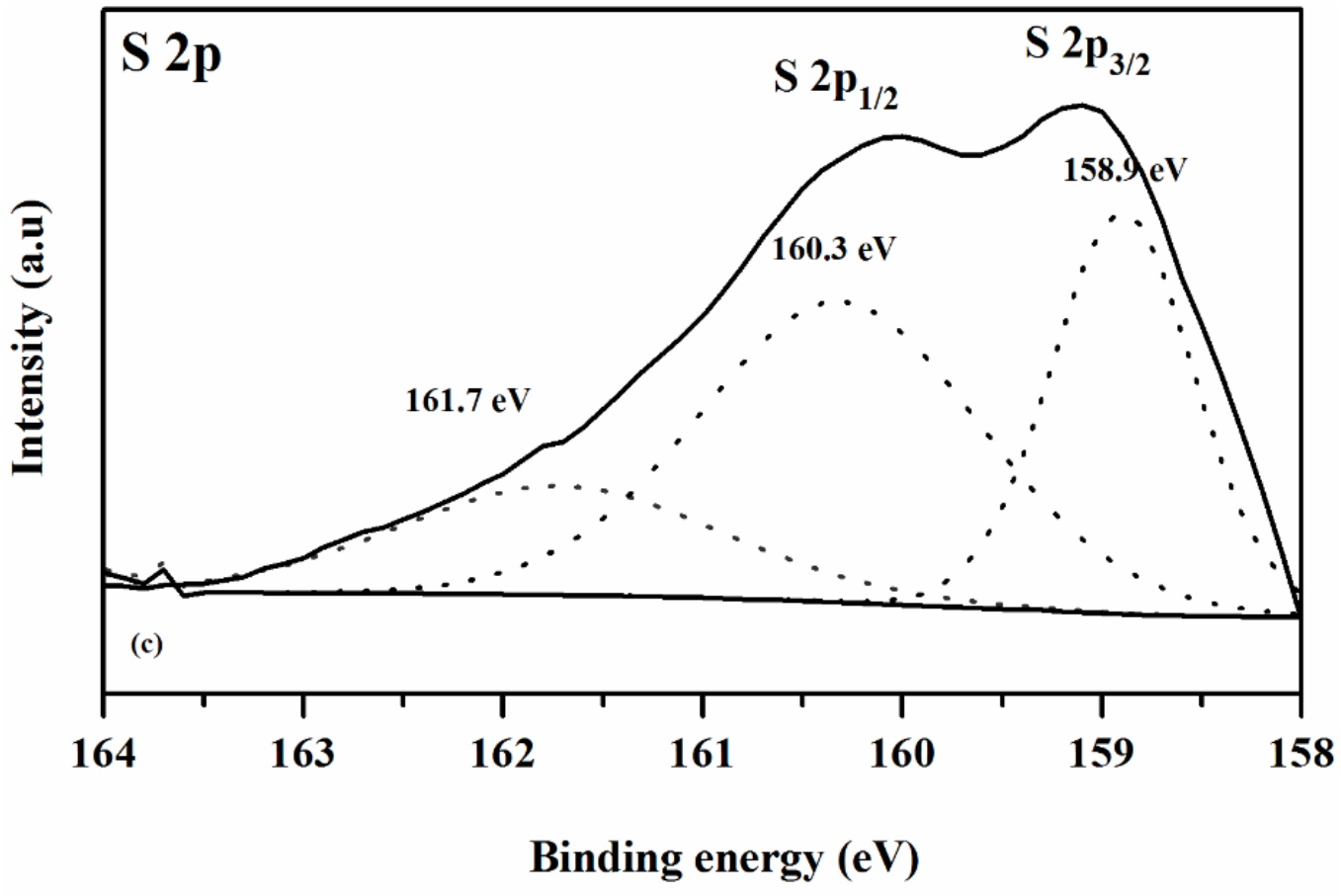

Fig. 7. High-resolution spectra of (a) Cu 2p core-level (b) Sb 3d core-level and (c) S 2p core level of Cu_3SbS_3 thin film annealed at 375 ^{0}C in an argon atmosphere.

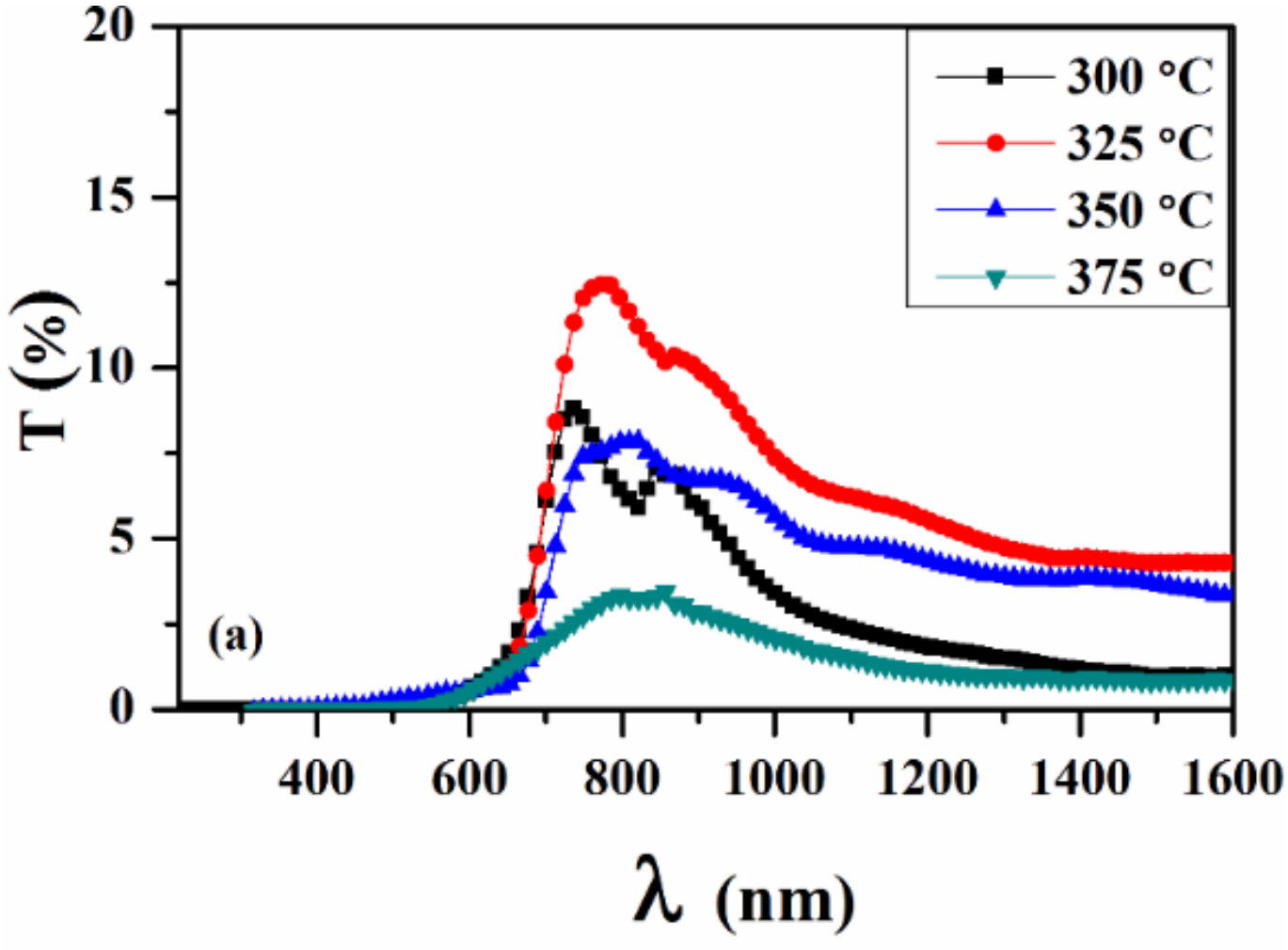
20
15
10
5
0
T (%)
(a)
300 °C
325 °C
350 °C
375 °C
400
600
800
1000
1200
1400
1600
λ (nm)

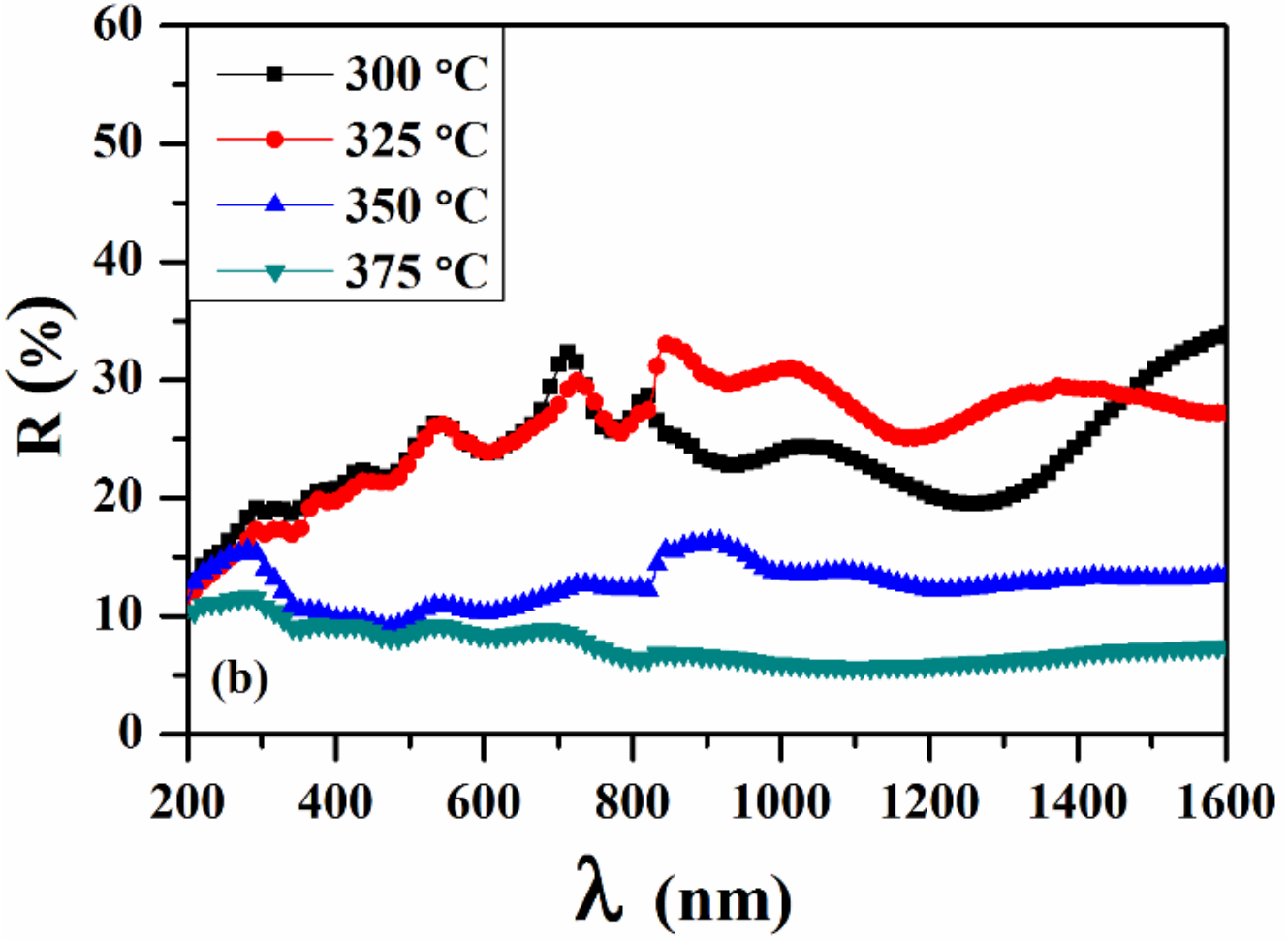

Fig. 8. Optical characteristics of the obtained Cu_3SbS_3 thin films (a) optical transmittance and (b) Reflectance.

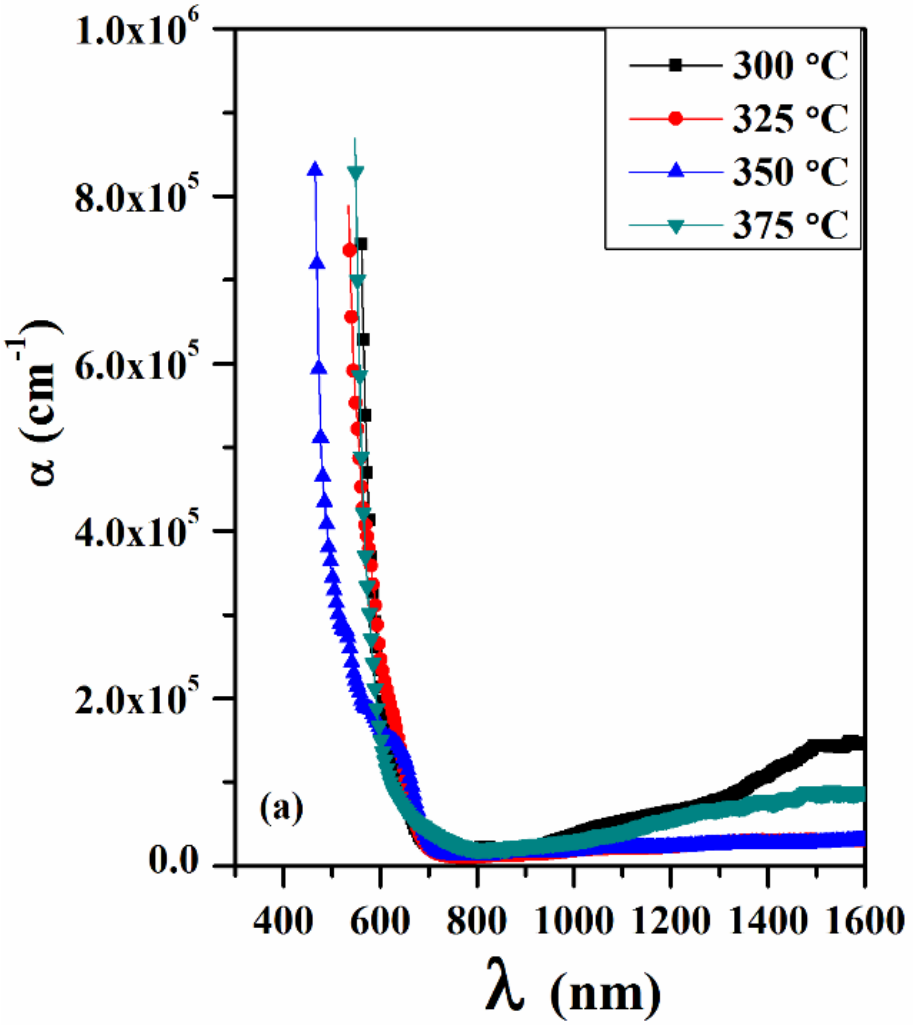
1.0x10^6
8.0x10^5
6.0x10^5
4.0x10^5
2.0x10^5
0.0
α (cm^-1)
300 °C
325 °C
350 °C
375 °C
(a)
400
600
800
1000
1200
1400
1600
λ (nm)

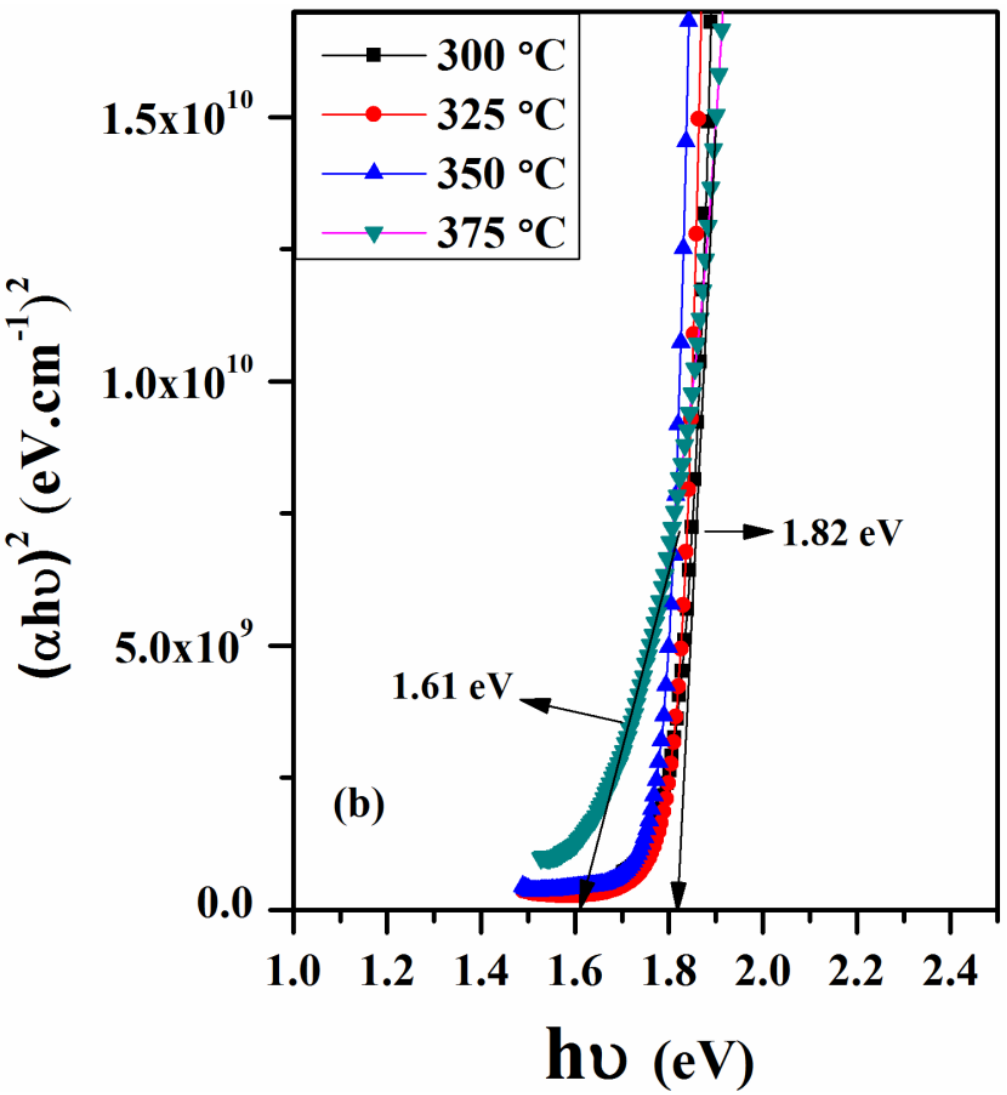

Fig. 9. (a) Optical absorption coefficient against wavelength and (b) Optical band gap energy (Tauc's plot)

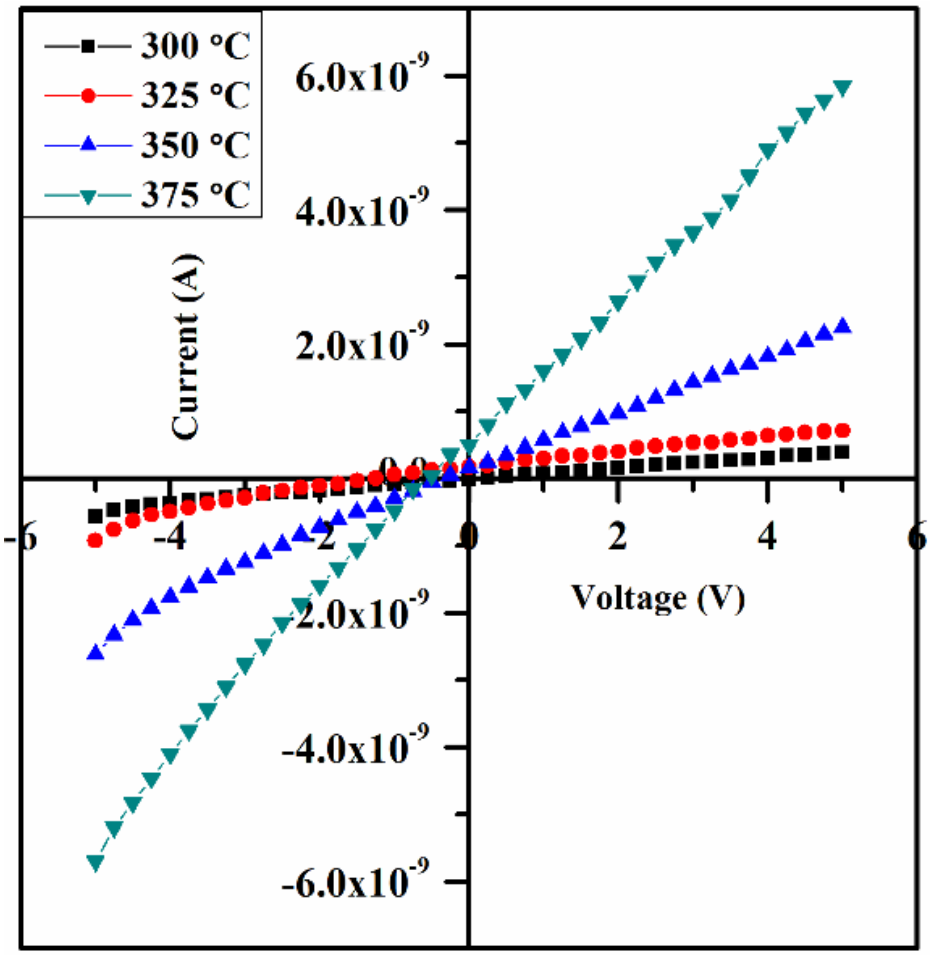

Fig. 10. The transverse current-voltage characteristics of the obtained Cu_3SbS_3 thin films.

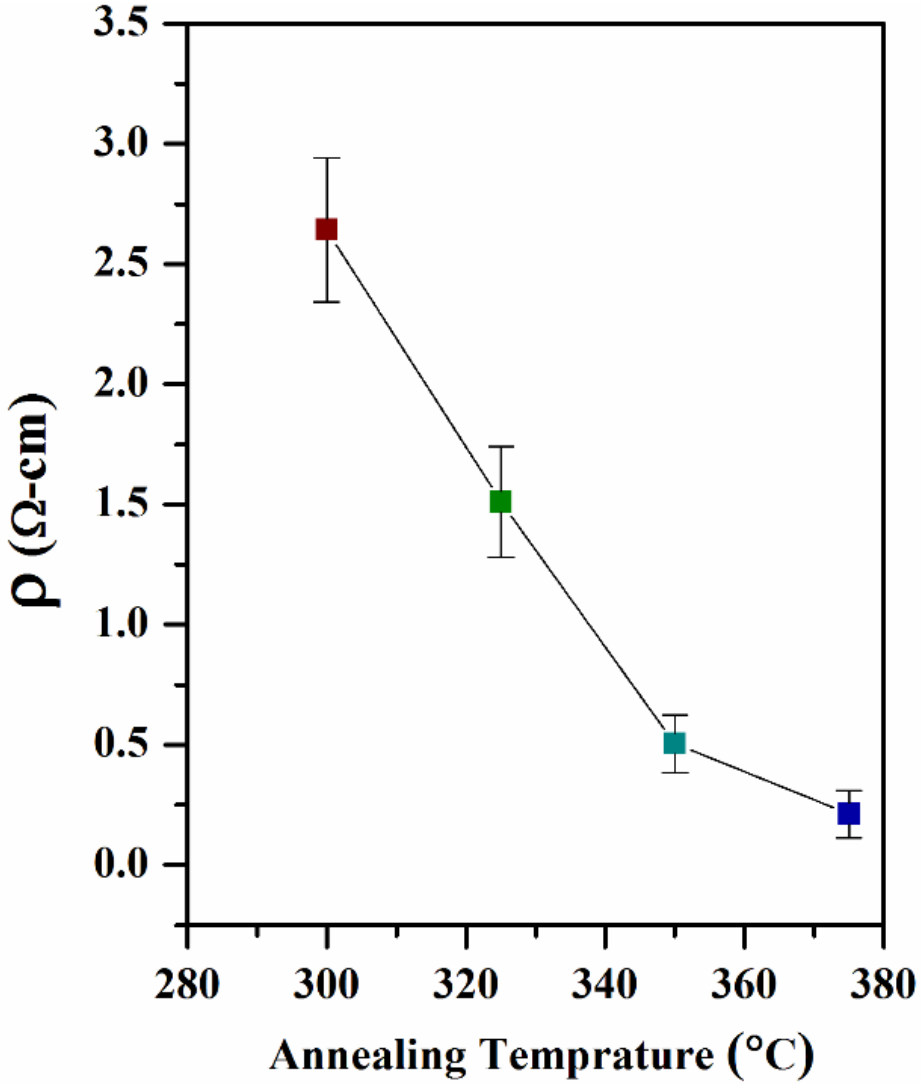

Fig. 11. Variation of resistivity with error bars as a function of annealing temperature.